Combining Experimental Isotherms, Minimalistic Simulations and a Model to Understand and Predict Chemical Adsorption onto Montmorillonite Clays

Supporting Information

Asuka A. Orr[1,2,†], Meichen Wang[3,†], Burcu Beykal[2], Hari S. Ganesh[2,4], Sara E. Hearon[3], Efstratios N. Pistikopoulos[1,2], Timothy D. Phillips[3,*], Phanourios Tamamis[1,2,5,*]

[1] Artie McFerrin Department of Chemical Engineering, Texas A&M University, College Station, Texas 77843-3122, United States.

[2] Texas A&M Energy Institute, Texas A&M University, College Station, Texas, 77843-3372, United States.

[3] Veterinary Integrative Biosciences Department, College of Veterinary Medicine and Biomedical Sciences, Texas A&M University, College Station, Texas 77843-3122, United States.

[4] Current Address: Indian Institute of Technology Gandhinagar, Palaj, Gandhinagar 382355, Gujarat, India.

[5] Department of Materials Science and Engineering, Texas A&M University, College Station, Texas, 77843-3003, United States.

[†]Equally contributing first authors

[*]Corresponding authors

Timothy D. Phillips: tphillips@cvm.tamu.edu

Phanourios Tamamis: tamamis@tamu.edu

Supporting Experimental Methods

Materials and Reagents

Calcium montmorillonite clay (CM) was purchased from Engelhard Chemical Corporation (and is now available from BASF in Lampertheim, Germany) with a total surface area as high as 850 m^2/g, an external surface area of approximately 70 m^2/g, and a cation exchange capacity (CEC) equal to 89.2 cmol/kg[1,2]. The generic formula for the CM clay is $(Ca)_{0.3}(Al,Mg)_2Si_4O_{10}(OH)_2 \cdot nH_2O$. Its chemical analysis by X-ray fraction spectroscopy (XRF) and X-ray powder diffraction (XRD) and its chemical morphology were previously published[3,4,5]. Reagents used in this study were all high-performance liquid chromatography (HPLC)-grade and purchased from VWR (Atlanta, GA). Analytical standards for chemicals were purchased from Sigma Aldrich (St. Louis, MO). Ultrapure deionized water (18.2 MΩ) was generated in the lab using an Elga automated filtration system (Woodridge, IL, USA) and used in all experiments.

Adsorption Isotherm Experiments

For the chemicals experimentally examined in this study, stock solutions were individually prepared by dissolving pure crystals into their corresponding solvents (Table 1), which were selected based on the hydrophobicity of the chemical. The concentrations of the stock solutions (Table S1) were set based on the octanol-water partitioning coefficients (Kow) so that precipitation was not a factor, and the optimal ratio of chemical/clay to reach saturation (equilibrium) on isotherm plots was investigated.

Following the preparation of the stock solutions, a concentration of 0.002% w/w of CM sorbent was exposed to an increasing concentration gradient (5–100%) of chemical solution. In

these studies, controls consisted of untreated solution (pure solvent as listed in Table 1), chemical solution without sorbent, and sorbent suspension without chemical. The control and test groups were capped and agitated at 1000 rpm on an IKA electric shaker (VIBRAX VXR basic, Werke, Germany) for 2 hours at a high temperature (37°C) and an ambient temperature (24°C) for thermodynamic experiments. This time was based on preliminary data suggesting that equilibrium of the surface interaction was reached within 30 min. In order to minimize contamination, only glassware was used for the preparation of plasticizers. All samples were then centrifuged at 2000 g for 20 min to separate the clay/chemical complex from solution and were detected by either ultraviolet (UV)/visible scanning spectrophotometry, HPLC, or liquid chromatography/tandem mass spectrometry (LC/MS/MS), as specified in the following section.

The amount adsorbed for each data point was calculated from the chemical concentration difference between test and control groups. These data were then plotted using Table-Curve two-dimensional (2D) and a computer program that was developed using Microsoft Excel to derive values for the variable parameters. Models including Langmuir and Freundlich were used to plot equilibrium isotherms from triplicate analysis based on the best fit for the adsorption data. Adsorption parameters coupled with the Gibbs free energy equation were used to calculate affinity (K_d) and adsorption free energy (ΔG in kJ/mol) (Table 1).

Analytical Chemistry

Phenol concentrations were analyzed using a SHIMADZU UV/visible scanning spectrometer (UV-1800, SHIMADZU Corporation, Kyoto, Japan)[6]. The concentrations were determined in supernatant samples that were placed in a quartz cuvette versus a blank and scanned

through the UV region of the electromagnetic spectrum (between 200 and 800 nm) to establish the wavelength for maximal absorption of phenol at 270 nm.

The concentration of DDT was analyzed using HPLC (Milford, MA, USA) with a Phenomenex luna 5u C18 column (250 × 4.6 mm, 5 μm) kept at an ambient temperature[7]. DDT was separated by 90% acetonitrile and 10% water as the mobile phase at 1.0 mL/min flow rate. Free DDT concentration in the supernatant was detected by a UV detector at 254 nm wavelength. The concentration of benzene and toluene were analyzed using HPLC with a SUPELCO LC-18 column (15 × 4.6 mm, 3 μm) at an ambient temperature[8]. The analysis was conducted using 70% acetonitrile and 30% water as the mobile phase at a flow rate of 1.0 mL/min. Benzene and toluene detection was programmed at 254 nm wavelength by the UV detector. The concentration of naphthalene, BBF (benzo(b)fluoranthene), and atrazine were analyzed on HPLC with a Waters Symmetry C18 (150 × 4.6 mm, 5 μm) at 30°C[9,10]. The mobile phase for PAHs was acetonitrile:water (60:40, v/v) at a flow-rate of 1.2 mL/min, and methanol:water (55:45, v/v) at 1.0 mL/min for atrazine. Detection was performed at 220 nm for naphthalene, 256 nm for BBF, and 230 nm for atrazine based on their maximum absorption. The injection volume was 20 μL for each sample. Breeze software was used to control the HPLC system and collect data. Breeze software was used to control the HPLC system and collect data.

The concentration of 2,4-D (2,4-dichlorophenoxyacetic acid), chlorpyrifos, BPS (bisphenol s), and BPF (bisphenol f) was analyzed using a Waters Acquity ultra performance LC/MS/MS (Milford, MA, USA) equipped with triple quadrupole and an Acquity BEH C18 column (2.1 × 50 mm, 1.7 μm) at 40°C[11,12]. For 2,4-D, BPS, and BPF, a gradient elution using water with 0.1% formic acid (eluent A) and acetonitrile (eluent B) was carried out (eluent B, 5% to start, and 5–100% linear gradient from 0.5 to 6 min) at a flow rate of 0.3 mL/min. A sample

volume of 20 μL was used for each analysis. MS analysis was performed with an electrospray ionization (ESI) interface and operated in a negative ion mode. The spray and cone voltages were maintained at 4 kV and 25 V, respectively. The source temperature was kept at 120°C. The mass spectrometer for precursor and product ions of 2,4-D, BPS, BPF, and phthalate were monitored at m/z 219 to 160.9, 227 to 212/133, 249 to 108.1/155.9, 199.1 to 105.1/93, and 279 to 205, respectively. Separation of chlorpyrifos was achieved using a mobile phase containing 10 mM ammonium acetate in water (eluent A) and 10 mM ammonium acetate in acetonitrile (eluent B) carried out at a flow rate of 0.6 mL/min and injection volume of 5 μL. The following gradient program was used for elution: 10% eluent B (0-1 min), 10–90% eluent B (1–8 min), 90% eluent B (8-10 min), and 90%-10% eluent B (10–11 min). MS analysis was operated in positive mode with capillary voltage at 5 kV and cone voltage at 30 V. The source temperature was kept at 350°C. Molecular ions of chlorpyrifos were monitored for precursor and products at m/z 350 to 198 and 96.9. For both methods, the mass spectrometer was operated under multiple reaction monitoring (MRM) mode. The unit mass resolution was used for ion mass analyzers. The enhanced product ion scan rate was 1000 amu/s, and the scan range was 106 to 396 amu. Nitrogen gas was used as the collision and curtain gas, and argon gas was used as the nebulizer and heater gas. Empower analyst software was used to control the LC/MS/MS system and acquire the data.

Standard concentrations of chemicals were spiked from 0.005 ppm to 20 ppm in the mobile phase and validated using calibration curves. Standard solutions were spiked before and after 2 hours of agitatation to determine non-specific binding.

Supporting Computational Methods

Minimalistic MD Simulations of Montmorillonite Clay in the Presence of Toxic Chemicals

The modeled CM clay had a stoichiometry of $(Si_4)^{IV}(Al_{1.67}Mg_{0.33})^{VI}O_{10}(OH)_2$. This model was generated by periodically replicating a 2.5 x 2.5 nm^2 montmorillonite clay layer extracted from the INTERFACE MD model database[13,14] to build a single 5 x 5 nm^2 layer. The single-layer montmorillonite clay model was solvated in a 90 × 90 × 21 $Å^3$ pre-equilibrated solvent box. For each of the 11 solvents (Table 1), prior to the solvation of the single-layer clay, short 10 ns MD simulations were performed to pre-equilibrate the solvent mixtures. The dimensions of the solvent box were selected such that, with the periodic boundary conditions applied in all MD simulations, the modeled clay would have infinite layers with an d_{001} spacing of 21 Å between each CM layer[15,16,17]. Subsequently, for each of the experimentally studied toxic chemical, 3 copies of the toxic chemical were placed within the simulation system comprising the CM clay layer and the corresponding pre-equilibrated solvent. All 3 copies of each toxic chemical were initially placed in the center of the simulation box and translated such that all copies were 10 Å normal from the clay interlayer surface (in the z-direction), with the first copy translated by 25 Å in the x-direction and 25 Å in the y-direction and the third copy translated by −25 Å in the x-direction and −25 Å in the y-direction. Thus, the final molar concentration of each toxic chemical within the simulation systems were 0.025 M per chemical-solvent combination (Table 1). The higher concentration used in the computational modeling compared to the experimental studies aimed to enhance the statistical sampling and accelerate the potential adsorption of the chemical compounds to the clay surface within the simulations similarly to our previous studies[15,17,18,18,19,20]. The initial molecular structures of each of the toxic chemicals were extracted from the ZINC database[21] or PubChem[22] if no structures were available from the ZINC database[21].

The CHARMM36 force field was used to model the water, acetonitrile, methanol, formic acid, acetate, and solvent molecules as well as Ca^{2+} counter ions[23]. Parameters and topologies extracted from the INTERFACE force field[13,14] were used for the CM clay. The INTERFACE force field can operate as an extension of common harmonic force fields including CHARMM, thereby enabling the simulation and study of systems comprising combinations of organic/biomolecular and inorganic interfaces[24,25,26,27] as well as montmorillonite[15,17,18,14]. All studied chemicals were parameterized using CGENFF[28,29].

Analogously to our previous studies[15,17,18], prior to each 30 ns MD simulation run, each system initially underwent 500 steps of steepest gradient descent minimization, 500 steps of Newton-Rapson minimization, and 500 steps of steepest descent minimization followed by a constrained 1 ns MD simulation equilibration stage. During the energy minimizations and 1 ns equilibration stage, the CM layer and the chemical compounds were constrained with a 1.0 kcal mol^{-1} $Å^{-1}$ harmonic constraint on all heavy atoms. Following energy minimization and equilibration, all constrains on the system were released except for light 0.1 kcal mol^{-1} $Å^{-1}$ harmonic constraint on aluminum atoms of the clay layers and the systems were simulated for 30 ns with a temperature of 300 K and a pressure of 1 atm. Hydrogen bond lengths were constrained using the SHAKE algorithm. MD simulation snapshots were extracted in 20 ps intervals for subsequent analysis. All MD simulations and setup were conducted in CHARMM[30].

Analysis of Minimalistic MD Simulations and Extraction of Data

Upon completion of the 30 ns all-atom minimalistic MD simulations of CM in the presence of the toxic chemicals, the simulation snapshots were analyzed to extract data for subsequent analysis. The first 10 ns of each simulation were considered as additional equilibration and the last

20 ns of each simulation were analyzed. Specifically, we calculated the electrostatic and van der Waals interaction energy for each instance a chemical compound was bound to the clay; a chemical compound was considered to be bound to the clay if any of its heavy atoms were within 3.5 Å of any heavy atom of the clay. The interaction energies were calculated between a bound chemical compound and the clay with all other components of the system (other compounds or solvent molecules) omitted. All energy calculations were performed in CHARMM[30] using infinite cutoffs. Importantly, the interaction energy values were used as inputs to the minimalistic model, described in the following section, to predict the absolute adsorption free energy of the toxic chemicals.

Evaluation of the Minimalistic Model

To evaluate the performance of the derived minimalistic model, we computed the model's Root Mean Square Error (RMSE) of the predicted free energies to the experimental free energies as well the sensitivity, specificity, and accuracy in identifying chemicals with high or low/no affinity for the CM clay through bootstrapping analysis. For the bootstrapping analysis, we used a 70:30 train:test random shuffled split using data for all chemicals in the study. This method involves resampling the data set by replacing the training data set (containing data corresponding to 24, or 70%, of the chemicals for this study) with a new training data set, randomly selected from the entire data set, after every bootstrap analysis iteration. This iterative process and random selection were repeated many times (10,000 times in this study) and the statistics of interest of each bootstrap population was calculated. The performance of the model was evaluated by calculating the average RMSE for the entire data set (35 adsorption free energy values) over all bootstrap iterations. The sensitivity of the model indicates its ability to correctly classify a chemical as a strong clay binder (positive) and is described by the following equation: Sensitivity

= (TP)/(TP + FN). The specificity of the model indicates its ability to correctly classify a chemical as a weak clay binder (negative) and is described by the following equation: Specificity = (TN)/(TN + FP). The accuracy of the model indicates its ability to correctly classify a chemical as either a strong or weak binder and is described by the following equation: Accuracy = (TN + TP)/(TN + TP + FN + FP). The statistics on the model's RMSE, sensitivity, specificity, and accuracy were collected over all 10,000 bootstrap analysis iterations. Additionally, the average values for parameters α and β derived from bootstrapping analysis are reported. The standard deviation of these values provides an estimate of the uncertainty associated with the average values derived based on a given sample for each model. Low/no affinity chemicals were defined as those having observed adsorption free energies greater than -3 kcal/mol, whereas high affinity chemicals were defined as those having observed adsorption free energies less than -3 kcal/mol.

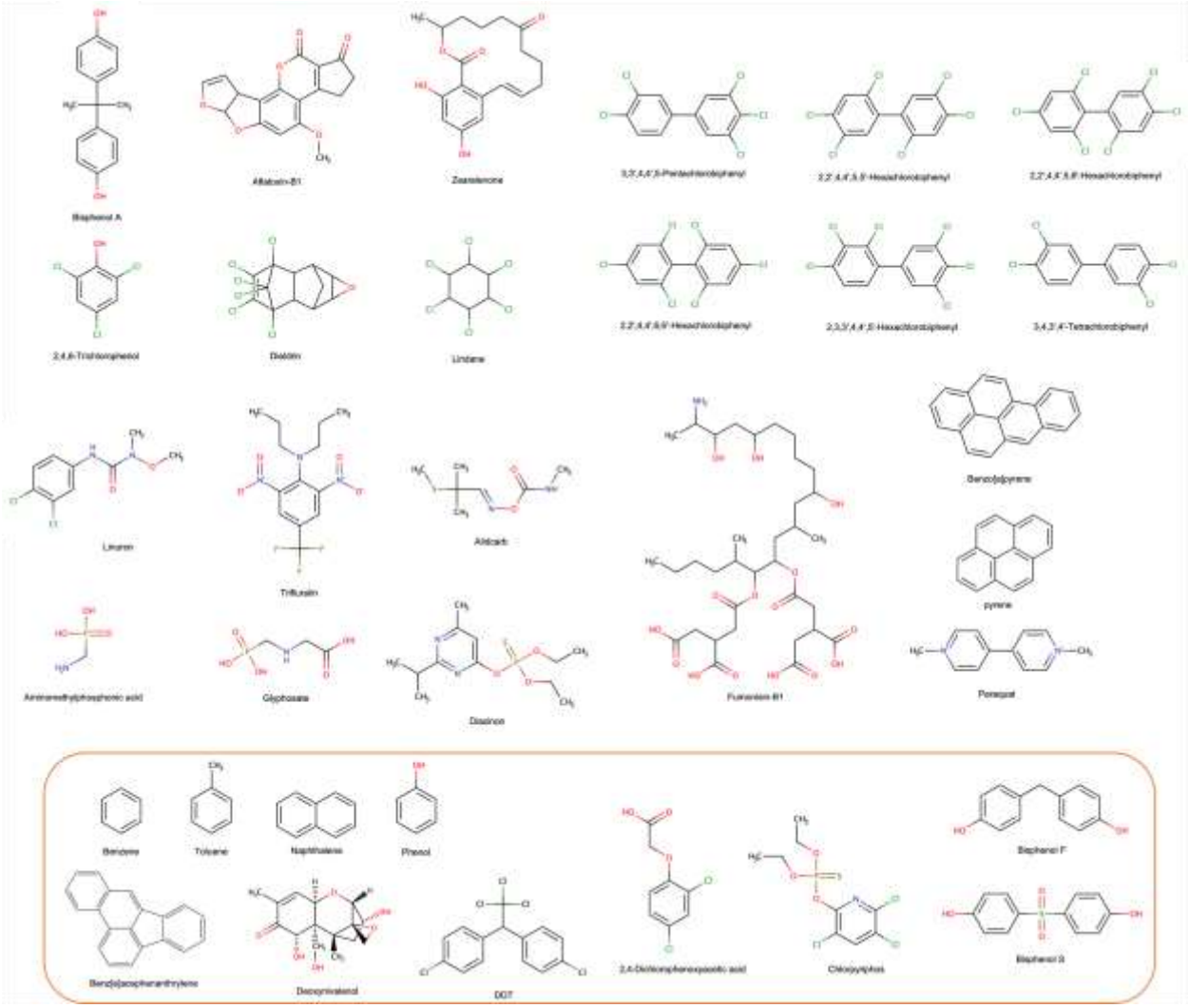

Figure S1. Structures of the chemical compounds investigated in this study. Structures within the orange box correspond to the 11 chemical compounds experimentally investigated in this study.

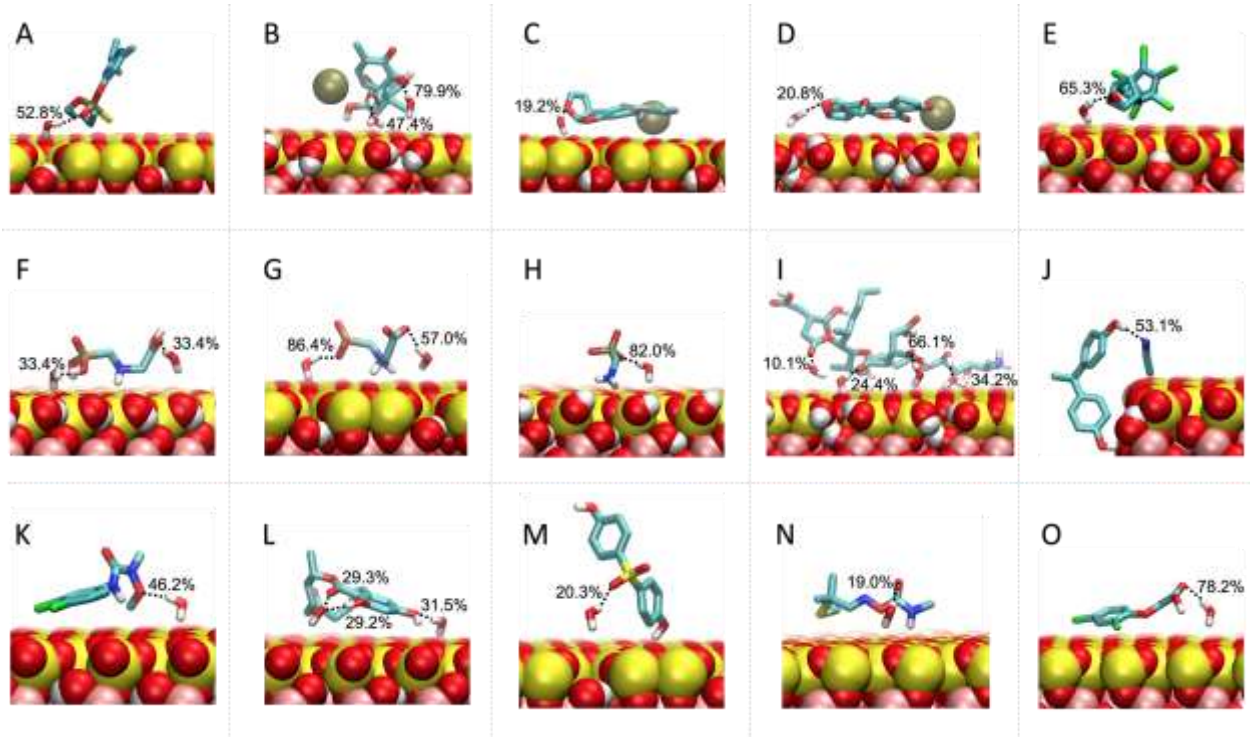

Figure S2. Molecular graphics images of the most prominent binding modes of adsorption for chemicals containing hydrogen bond donors/acceptors in their chemical structures with free energies less than -3 kcal/mol. Solvent mediated interactions are indicated with black dotted lines. The percent propensity of the solvent mediated interactions formed within the displayed most prominent binding modes are shown for each solvent mediated interaction. Chemicals include (A) diazinon, (B) deoxynivalenol, (C) aflatoxin-B1 at pH 7, (D) aflatoxin-B1 at pH 2, (E) dieldrin, (F) glyphosate at pH 2, (G) glyphosate at pH 7, (H) aminomethylphosphonic acid, (I) fumonisin-B1, (J) bisphenol A, (K) linuron, (L) zearalenone, (M) bisphenol S, (N) aldicarb, and (O) 2,4-dichlorophenoxyacetic acid are shown in licorice representation with non-polar hydrogens omitted for clarity. Montmorillonite and Ca^{2+} ions are shown in van der Waals representation.

Table S1. List of calibration curve coefficients and limits of detection of target compounds.

Chemical	**Correlation coefficient (r^2)**	**Limit of detection(ppb)**
Glyphosate	0.9904	125
Dieldrin	0.99	250
DDT	0.9999	500
2,4-D	0.9967	1000
PCBs	>0.999	500
Aldicarb	0.9987	33.3
Naphthalene	0.9999	1000
Linuron	0.9999	5
Aflatoxin-B1	0.9911	200
Diazinon	0.9997	12.5
Zearalenone	0.99	200
Fumonisin-B1	0.9933	625
Paraquat	0.9935	10
2,4,6-Trichlorophenol	0.9992	500
Bisphenols	>0.99	100
Lindane	0.991	5
Phenol	0.9997	625
Toluene	0.9995	125
Chlorpyrifos	0.9945	250
Atrazine	0.9932	100
Benzene	0.9988	250
Trifluralin	0.9999	100
AMPA	0.9911	125
BBF	0.9921	500
BaP	0.9944	0.032

Table S2. Percent propensities of the most prominent binding modes of the studied chemicals displayed in Figure 4.

Chemical	Solvent	Propensity of Most Prominent Binding Mode (%)
3,3',4,4',5-Pentachlorobiphenyl (PCB126)	acetonitrile	90.2
3,4,3',4'-Tetrachlorobiphenyl (PCB77)	acetonitrile	85.1
2,2',4,4',5,5'-Hexachlorobiphenyl (PCB153)	acetonitrile	91.0
Bisphenol A	acetonitrile	94.5
2,3,3',4,4',5'-Hexachlorobiphenyl (PCB157)	acetonitrile	76.3
2,2',4,4',6,6'-Hexachlorobiphenyl (PCB155)	acetonitrile	78.4
Lindane	acetonitrile:water 50:50	95.6
Naphthalene	acetonitrile:water 60:40	96.4
Benz[e]acephenanthrylene	acetonitrile:water 60:40	94.1
Dieldrin	acetonitrile:water 65:35	63.0
Linuron	acetonitrile:water 65:35	55.6
Trifluralin	acetonitrile:water 70:30	61.2
Bisphenol S	acetonitrile:water 80:20	67.8
Benzo[a]pyrene	acetonitrile:water 90:10	93.0
2,4-Dichlorophenoxyacetic acid	acetonitrile:water 90:10	72.1
Clofenotane (DDT)	acetonitrile:water 90:10	55.1
Pyrene	MeOH:water 90:10	82.7
Deoxynivalenol (vomitoxin)	water-pH2	59.8
Glyphosate	water-pH2	56.3
Fumonisin-B1	water-pH2	54.0
Aflatoxin-B1	water-pH2	77.1
2,4,6-Trichlorophenol	water-pH2	80.5
Diazinon	water-pH7	77.3
Paraquat	water-pH7	95.4
Aflatoxin-B1	water-pH7	70.1
Phenol	water-pH7	96.0
Aminomethylphosphonic acid	water-pH7	89.2
Glyphosate	water-pH7	70.8
Chlorpyriphos	water-pH7	72.2
Zearalenone	water-pH7	55.0
Aldicarb	water-pH7	59.1

Supporting References

[1] Grant, P. G.; Phillips, T. D. Isothermal adsorption of aflatoxin B(1) on HSCAS clay. *J. Agric. Food Chem.* **1998**, *46*, 599–605.

[2] Wang, M.; Hearon, S. E.; Phillips, T. D. Development of enterosorbents that can be added to food and water to reduce toxin exposures during disasters. *J. Environ. Sci. Health B* **2019**, *54*, 514–524.

[3] Wang, M.; Hearon, S. E.; Phillips, T. D. A high capacity bentonite clay for the sorption of aflatoxins. *Food Addit. Contam. Part A Chem. Anal. Control Expo. Risk Assess.* **2020**, *37*, 332–341.

[4] Marroquín-Cardona, A.; Deng, Y.; Garcia-Mazcorro, J.; Johnson, N. M.; Mitchell, N.; Tang, L.; Robinson, A.; Taylor, J.; Wang, J. S.; Phillips, T. D. Characterization and safety of uniform particle size novasil clay as a potential aflatoxin enterosorbent. *Appl. Clay Sci.* **2011**, *54*, 248–257.

[5] Wang, M.; Chen, Z.; Rusyn, I.; Phillips, T. D. Testing the efficacy of broad-acting sorbents for environmental mixtures using isothermal analysis, mammalian cells, and H. vulgaris. *J. Hazard. Mater.* **2020**, 124425.

[6] Martynoff, M. Note de laboratoire: Spectres d'absorption de quelques p-quinones. *Bull. Soc. Chim. Fr.* **1949**, *16*, 258–261.

[7]Determination of DDT by C18 RP-HPLC. https://spectralabsci.com/wp-content/uploads/PDFFiles/Determination%20of%20DDT%20by%20C18%20RP.pdf.

[8] Abdulrahman Bahrami; Hosien Mahjub; Marzieh Sadeghian; Farideh Golbabaei. Determination of Benzene, Toluene and Xylene (BTX) Concentrations in Air Using HPLC Developed Method Compared to Gas Chromatography. *International Journal of Occupational Hygiene* **1970**, *3*.

[9] Jacomini, A. E.; Bonato, P. S.; Avelar, W. E. P. HPLC method for the analysis of atrazine in freshwater bivalves. *J. Liq. Chromatogr. Relat. Technol.* **2003**, *26*, 1885–1894.

[10] EPA method 550.1 Determination of polycyclic aromatic hydrocarbons in drinking water by liquid-solid extraction and HPLC with coupled ultraviolet and fluorescence detection, 1990. https://www.o2si.com/docs/epa-method-550.1.pdf

[11] Wittrig, B. Comprehensive Pesticide Residue Analysis by LC-MS/MS Using an Ultra Aqueous C18 Column, 2019. Restek Pure Chromatography. https://www.restek.com/adv004

[12] Hindle, R. Analysis of 2,4-D, 2,4,5-T, Bromoxynil, and Dinoseb Herbicides in Drinking Water Using the Agilent 6495 Triple Quadrupole LC/MS, 2015. Agilent Technologies. http://hpst.cz/sites/default/files/attachments/5991-5731en.pdf

[13] Heinz, H.; Lin, T.-J.; Mishra, R. K.; Emami, F. S. Thermodynamically consistent force fields for the assembly of inorganic, organic, and biological nanostructures: the INTERFACE force field. *Langmuir* **2013**, *29*, 1754–1765.

[14] Heinz, H.; Koerner, H.; Anderson, K. L.; Vaia, R. A.; Farmer, B. L. Force Field for Mica-Type Silicates and Dynamics of Octadecylammonium Chains Grafted to Montmorillonite. *Chem. Mater.* **2005**, *17*, 5658–5669.

[15] Wang, M.; Orr, A. A.; He, S.; Dalaijamts, C.; Chiu, W. A.; Tamamis, P.; Phillips, T. D. Montmorillonites can tightly bind glyphosate and paraquat reducing toxin exposures and toxicity. *ACS Omega* **2019**, *4*, 17702–17713.

[16] Orr, A. A.; He, S.; Wang, M.; Goodall, A.; Hearon, S. E.; Phillips, T. D.; Tamamis, P. Insights into the interactions of bisphenol and phthalate compounds with unamended and carnitine-amended montmorillonite clays. *Comput. Chem. Eng.***2020**, *143*, 107063.

[17] Wang, M.; Orr, A. A.; Jakubowski, J. M.; Bird, K. E.; Casey, C. M.; Hearon, S. E.; Tamamis, P.; Phillips, T. D. Enhanced adsorption of per- and polyfluoroalkyl substances (PFAS) by edible, nutrient-amended montmorillonite clays. *Water Res.***2020**, *188*, 116534.
[18] Tamamis, P.; Adler-Abramovich, L.; Reches, M.; Marshall, K.; Sikorski, P.; Serpell, L.; Gazit, E.; Archontis, G. Self-assembly of phenylalanine oligopeptides: insights from experiments and simulations. *Biophys. J.* **2009**, *96*, 5020–5029.
[19] Chen, Y.; Orr, A. A.; Tao, K.; Wang, Z.; Ruggiero, A.; Shimon, L. J. W.; Schnaider, L.; Goodall, A.; Rencus-Lazar, S.; Gilead, S.; et al. High-Efficiency Fluorescence through Bioinspired Supramolecular Self-Assembly. *ACS Nano* **2020**, *14*, 2798–2807.
[20] Tao, K.; Chen, Y.; Orr, A. A.; Tian, Z.; Makam, P.; Gilead, S.; Si, M.; Rencus-Lazar, S.; Qu, S.; Zhang, M.; et al. Enhanced Fluorescence for Bioassembly by Environment-Switching Doping of Metal Ions. *Adv. Funct. Mater.* **2020**, *30*.
[21] Sterling, T.; Irwin, J. J. ZINC 15--Ligand Discovery for Everyone. *J. Chem. Inf. Model.* **2015**, *55*, 2324–2337.
[22] Kim, S.; Chen, J.; Cheng, T.; Gindulyte, A.; He, J.; He, S.; Li, Q.; Shoemaker, B. A.; Thiessen, P. A.; Yu, B.; et al. PubChem 2019 update: improved access to chemical data. *Nucleic Acids Res.* **2019**, *47*, D1102–D1109.
[23] Huang, J.; MacKerell, A. D. CHARMM36 all-atom additive protein force field: validation based on comparison to NMR data. *J. Comput. Chem.* **2013**, *34*, 2135–2145.
[24] Pacella, M. S.; Gray, J. J. A benchmarking study of peptide–biomineral interactions. *Cryst. Growth Des.* **2018**, *18*, 607–616.
[25] Emami, F. S.; Puddu, V.; Berry, R. J.; Varshney, V.; Patwardhan, S. V.; Perry, C. C.; Heinz, H. Prediction of specific biomolecule adsorption on silica surfaces as a function of ph and particle size. *Chem. Mater.* **2014**, *26*, 5725–5734.
[26] Heinz, H.; Vaia, R. A.; Farmer, B. L. Interaction energy and surface reconstruction between sheets of layered silicates. *J. Chem. Phys.* **2006**, *124*, 224713.
[27] Makó, É.; Kovács, A.; Ható, Z.; Zsirka, B.; Kristóf, T. Characterization of kaolinite-ammonium acetate complexes prepared by one-step homogenization method. *J. Colloid Interface Sci.* **2014**, *431*, 125–131.
[28] Vanommeslaeghe, K.; MacKerell, A. D. Automation of the CHARMM General Force Field (CGenFF) I: bond perception and atom typing. *J. Chem. Inf. Model.* **2012**, *52*, 3144–3154.
[29] Vanommeslaeghe, K.; Raman, E. P.; MacKerell, A. D. Automation of the CHARMM General Force Field (CGenFF) II: assignment of bonded parameters and partial atomic charges. *J. Chem. Inf. Model.* **2012**, *52*, 3155–3168.
[30] Brooks, B. R.; Brooks, C. L.; Mackerell, A. D.; Nilsson, L.; Petrella, R. J.; Roux, B.; Won, Y.; Archontis, G.; Bartels, C.; Boresch, S.; et al. CHARMM: the biomolecular simulation program. *J. Comput. Chem.* **2009**, *30*, 1545–1614.